Absorption coefficients and exciton oscillator strengths in AlGaAs-GaAs superlattices

W. T. Masselink,* P. J. Pearah,† J. Klem,† C. K. Peng,‡ and H. Morkoç†
Coordinated Science Laboratory, University of Illinois at Urbana-Champaign, 1101 West Springfield Avenue, Urbana, Illinois 61801

G. D. Sanders* and Yia-Chung Chang*
Materials Research Laboratory, University of Illinois at Urbana-Champaign, 104 South Goodwin Avenue, Urbana, Illinois 61801

(Received 19 June 1985)

We have experimentally determined the absolute optical-absorption coefficients and exciton oscillator strengths in AlGaAs-GaAs superlattices at liquid-helium temperatures. We find that although the magnitude of the band-to-band absorption coefficient is essentially independent of the quantum-well width, the absorption coefficient due to exciton absorption is greatly enhanced as the well width becomes smaller. The absorption energies and exciton oscillator strengths are compared to theoretical calculations and shown to be in very good agreement. We find that the oscillator strength per unit volume is proportional to $1/L^2$ in narrow wells. The effects due to coupling between wells was also investigated by the comparison of structures with barriers of 100 Å to those with barriers of only 25 Å. The subband energies in the coupled wells decreased from their values in uncoupled wells in quantitative agreement with our calculations while the oscillator strength also decreased.

For a number of years valuable information on quantum-size effects in semiconductor superlattices has been obtained through optical-absorption measurements.[1] Original studies of optical absorption in GaAs-$Al_xGa_{1-x}As$ superlattices showed clear evidence of multiple subbands in the GaAs wells due to quantum confinement of electrons and holes.[2–4] Splittings of absorption peaks were resolved corresponding to distinct heavy- and light-hole valence-band edges[2] and to coupling between adjacent wells.[3] Another important quantum-size effect, the increase in binding energy of free excitons, was apparent already in early studies.[5] Subsequent absorption and excitation-spectroscopy studies in GaAs-AlGaAs superlattices have allowed a more direct determination of the exciton binding energies.[6–8] More recently, new effects have been observed in superlattice absorption with an applied electric field.[9]

In all of these previous absorption experiments, the absorption intensity has been reported only in arbitrary units. This is, of course, perfectly adequate for studying the transition energies; on the other hand, both as a further check of theoretical models and as a guide for further optical experiments (such as determining penetration depth of Raman probes or for photopumped laser studies), a quantitative absorption study is desirable. In this study we have measured the absolute absorption coefficient as a function of the photon energy for multiple-quantum-well samples with well widths ranging from 40 to 315 Å. From these absorption measurements, a large number of transitions were observed, many of them violating the $\Delta n=0$ selection rule. The absorption itself was dominated by free-exciton absorption, allowing measurements of absolute exciton oscillator strengths. Both energy positions of absorption peaks as well as relative absorption coefficients and exciton oscillator strengths are compared with theory.

The GaAs-$Al_xGa_{1-x}As$ multiple-quantum-well (MQW) structures studied here were grown by molecular-beam epitaxy (MBE) on n^+ or semi-insulating ⟨100⟩ GaAs substrates. Substrate preparations and MBE growth of the quantum wells were generally typical. The growth sequence consisted of 0.3—0.5 μm of GaAs buffer, 500 Å of AlAs, and then the MQW structure. A dimeric arsenic (As_2) flux used during growth was generated by a specially designed cracking furnace.[10] To ensure greater uniformity across the substrate, the substrate was continually rotated during growth. The total thickness of the MQW structures ranged from 0.9 to 2.2 μm. Most of these structures had barrier widths (L_b) of 100 Å with varying well widths (L_z). Two of the structures were grown with thinner barriers ($L_b=25$ with $L_z=90$ and 150 Å) to study the effects of coupling between wells. AlAs mole fractions in the barriers were near 0.25 in all cases. A very thin etch-stop layer (500 Å of AlAs) was included between the MQW and the GaAs buffer layer to facilitate the preparation of samples for optical-transmission measurements.

Optical-transmission samples were fabricated by permanently mounting the sample onto a clear glass cover slide using a transparent cyanoacrylate adhesive. After lapping the substrate to a thickness of approximately 50 μm, a circle with diameter of 1 mm was photolithographically defined. The substrate was then etched away in this circle using an etch (H_2O_2:NH_4OH, 96:4) which selectively etches GaAs but not AlAs. Thus in this circular area only the MQW structure and the etch stop remain. Upon completion, transmitted light was clearly visible. All samples were carefully examined under high magnification to ensure that no cracks or pinholes were present.

Optical measurements were performed with samples cooled to <3 K in a Janis optical cryostat. The transmission spectra were measured using a broadband 100-W

tungsten lamp as the light source. Transmitted light was focused onto the entrance slit of a 1.26-m-focal-length grating spectrometer; the dispersed light was detected with a cooled GaAs photocathode photomultiplier. Figure 1 depicts a typical transmission spectrum for a MQW sample with 210-Å wells and 100-Å barriers. The dips in transmission (which correspond to absorption peaks) are labeled according to their probable origin. (Throughout this paper, the notation LHm-CBn denotes an exciton whose wave function is derived from states which at $k=0$ have the character of the mth light-hole and nth electron subbands; similarly, HHm-CBn denotes an exciton with the character of the mth heavy-hole and nth electron subbands.)

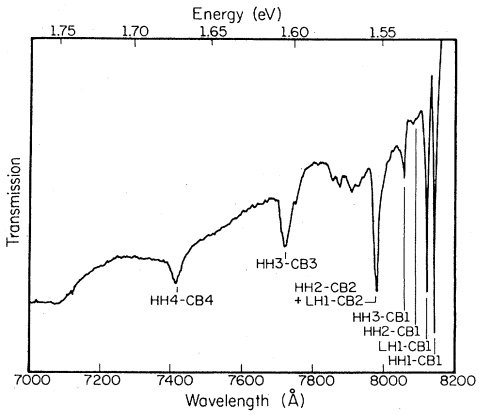

FIG. 1. Transmission spectrum of a GaAs-$Al_{0.25}Ga_{0.75}As$ multiple-quantum-well sample with 210-Å wells and 100-Å barriers.

The subband energies can easily be calculated within the effective-mass approximation by solving the one-dimensional Schrödinger equation for a particle in a finite well. By correctly considering the boundary conditions, effects due to mass differences and interwell coupling may be easily included. The effective-mass Schrödinger equation for a particle (electron or hole) of mass m_w in the well of width L_z is

$$-\left[\frac{\hbar^2}{2m_w}\right]\frac{d^2}{dz^2}\psi=E\psi ,$$

where ψ is the envelope wave function for the particle in the well and E is the energy measured with respect to the bottom of the well. The solutions at $k=0$ to this equation with definite parity are

$$\psi_g=A_g\cos\left[\left[\frac{2m_wE}{\hbar^2}\right]^{1/2}z\right] \quad \text{(even parity)}$$

and

$$\psi_u=A_u\sin\left[\left[\frac{2m_wE}{\hbar^2}\right]^{1/2}z\right] \quad \text{(odd parity)} .$$

In the barrier material, the effective-mass Schrödinger equation is

$$-\left[\frac{\hbar^2}{2m_b}\right]\frac{d^2}{dz^2}\Phi=(E-V)\Phi ,$$

where m_b is the mass in the barrier, V is the barrier-height energy, E is again the energy measured with respect to the bottom of the well, and Φ is the envelope wave function for the particle in the barrier. Since $E<V$, the solutions to this equation with definite parity are

$$\Phi_g=B_g\cosh\left[\left[\frac{2m_b(V-E)}{\hbar^2}\right]^{1/2}\left[z-\frac{L_z+L_b}{2}\right]\right] \quad \text{(even parity)}$$

and

$$\Phi_u=B_u\sinh\left[\left[\frac{2m_b(V-E)}{\hbar^2}\right]^{1/2}\left[z-\frac{L_z+L_b}{2}\right]\right] \quad \text{(odd parity)} ,$$

where L_z is again the width of the well and L_b is the width of the barrier. One boundary between well and barrier occurs at $z=L_z/2$. At this boundary the particle current and probability must remain constant. Thus, for even parity,

$$\psi_g(L_z/2)=\Phi_g(L_z/2) \quad \text{and} \quad \frac{1}{m_w}\frac{d}{dz}\psi_g=\frac{1}{m_b}\frac{d}{dz}\Phi_g .$$

Solving,

$$A_g\cos\left[\left[\frac{2m_wE}{\hbar^2}\right]^{1/2}\frac{L_z}{2}\right]=B_g\cosh\left[\left[\frac{2m_b(V-E)}{\hbar^2}\right]^{1/2}\left[-\frac{L_b}{2}\right]\right]$$

and

$$-A_g\frac{1}{m_w}\left[\frac{2m_wE}{\hbar^2}\right]^{1/2}\sin\left[\left[\frac{2m_wE}{\hbar^2}\right]^{1/2}\frac{L_z}{2}\right]=B_g\frac{1}{m_b}\left[\frac{2m_b(V-E)}{\hbar^2}\right]^{1/2}\sinh\left[\left[\frac{2m_b(V-E)}{\hbar^2}\right]^{1/2}\left[\frac{-L_b}{2}\right]\right] ,$$

so

$$\frac{1}{m_w}\left[\frac{2m_wE}{\hbar^2}\right]^{1/2}\tan\left[\left[\frac{2m_wE}{\hbar^2}\right]^{1/2}\frac{L_z}{2}\right]=\frac{1}{m_b}\left[\frac{2m_b(V-E)}{\hbar^2}\right]^{1/2}\tanh\left[\left[\frac{2m_b(V-E)}{\hbar^2}\right]^{1/2}\frac{L_b}{2}\right],$$

or

$$(E/m_w)^{1/2}\tan\left[\left[\frac{2m_wE}{\hbar^2}\right]^{1/2}\frac{L_z}{2}\right]=[(V-E)/m_b]^{1/2}\tanh\left[\left[\frac{2m_b(V-E)}{\hbar^2}\right]^{1/2}\frac{L_b}{2}\right]. \quad (1)$$

This transcendental equation can be easily solved graphically or numerically to determine E for even-parity states.

Similarly,

$$(E/m_w)^{1/2}\coth\left[\left[\frac{2m_wE}{\hbar^2}\right]^{1/2}\frac{L_z}{2}\right]=-[(V-E)/m_b]^{1/2}\coth\left[\left[\frac{2m_b(V-E)}{\hbar^2}\right]^{1/2}\frac{L_b}{2}\right] \quad (2)$$

can be solved to determine E for odd-parity states.

We solved these equations for both electrons and holes, taking the electron effective mass to be $0.067m_0$ in the GaAs wells and $(0.067+0.083x)m_0$ in the $Al_xGa_{1-x}As$ barriers.[11] The hole masses were defined in terms of the Luttinger parameters given by Lawaetz[12] in both GaAs and AlGaAs. The heavy-hole mass is

$$m_H=m_e/(\gamma_1-2\gamma_2),$$

and the light-hole mass is

$$m_L=m_e/(\gamma_1+2\gamma_2).$$

For the alloy we used a linear interpolation for γ_1 and γ_2 between GaAs and AlAs. The barrier height V was deduced by considering 65% of the band-gap discontinuity to be in the conduction band and 35% in the valence band:[13,14] The band-gap discontinuity between the GaAs and the $Al_xGa_{1-x}As$ was taken to be $1.247x$ eV.[11] The energy solutions to Eqs. (1) and (2) are not extremely sensitive to band-gap discontinuity; thus, given some uncertainty in the hole masses, AlAs mole fraction (x), and exact value of the well width, these measurements are not extremely well suited for determining the band alignments.

The observed transmission dips in Fig. 1 are due to exciton absorption, which occurs at energies given by

$$E_{n,m}(L_z)=E_g+E_{n,e}(L_z)+E_{m,h}(L_z)-E^B_{n,m}(L_z),$$

where E_g is the band gap of the GaAs, $E_{n,e}(L_z)$ is the solution to Eq. (1) or (2) for the electron and n is the subband index, $E_{m,h}(L_z)$ is the solution to Eq. (1) or (2) for the heavy or light hole, and m is the subband index, and $E^B_{n,m}(L_z)$ is the binding energy for the exciton associated with the n and m subbands and well width L_z. The exciton binding energy is determined from a variational calculation such as that described in Ref. 15.

The exciton absorption energies calculated as described above are plotted as functions of well width in Fig. 2 for 100-Å $Al_{0.25}Ga_{0.75}As$ barriers. Also depicted are the observed absorption energies from Fig. 1 and from other structures similarly measured. As one can see from Fig. 2, there is good agreement between the measured and calculated energies. Although for most of the transitions the electron subband index is the same as either the light-hole or heavy-hole subband index, there are a number of relatively strong transitions where this is not true. The reason for this is valence subband coupling, which will be discussed quantitatively later in the paper. In addition to the good agreement between experiment and theory for both the allowed and "forbidden" transitions, this experiment is unusual in the large number of observed exciton transitions—up to 12 in a single structure.

Besides measuring the absorption energies, we also determined the absolute absorption coefficients for all spectra as functions of photon energies. The absorption

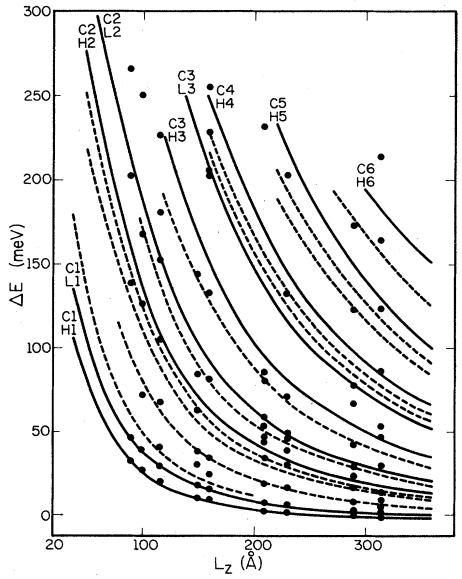

FIG. 2. Measured and calculated exciton-absorption energies as functions of well width for GaAs-$Al_{0.25}Ga_{0.75}As$ multiple-quantum-well samples with 100-Å barriers. The experimental data are solid circles.

spectra were obtained from transmission data using the well-known relation

$$T=\frac{(1-R)^2e^{-\alpha d}}{1-R^2e^{-2\alpha d}}\ , \tag{3}$$

where T is the quotient of the light transmitted through the mounted sample (including glass cover slide) and that transmitted through the glass cover slide with no sample and with the same incident light in both cases. The parameters α and d are the absorption coefficient and sample thickness, respectively. Values of R were obtained by setting $\alpha=0$ at energies much lower than the value $E_g+E_{1,e}+E_{1,hh}$. These values were near 0.3, which is typical of the bulk materials.[16] Reflections at the heterointerfaces have been ignored, since the discontinuity in the index of refraction is quite small. Using published data[17] for $h\nu=1.74$ eV and $x=0.38$, for example, the reflectance at the heterointerface, $R_2=(n_2-n_1)^2/(n_2+n_1)^2$, is on the order of 10^{-3}. This approach has been used previously in the analysis of GaAs-AlGaAs heterolayer transmission data.[18]

In MQW structures the definition of the thickness d is not entirely straightforward. Ideally, d is the thickness of the material which is absorbing the light. If we are dealing with decoupled wells, that is, wells separated by thick barriers, then d should be the total thickness of the wells only. This is necessary because increasing the barrier thickness should not affect the optical properties (below the barrier-height energy) and, therefore, α should remain unchanged. In coupled wells, however, α will depend both on well and barrier thickness. In such a system it may be more sensible to consider the superlattice to be one (anisotropic) single material and define d to be the thickness of the entire superlattice. For the structures in this study with 100-Å barriers, we considered the wells to be substantially decoupled and therefore took d to be the thickness of the wells only. The coupled wells will be discussed later in the paper.

Figure 3(a) shows the absorption spectrum deduced from Fig. 1 as described. Superimposed on this figure is a calculated absorption spectrum for the same structure.

The theoretically predicted absorption spectrum is based on a multiband effective-mass model described in Ref. 15. The effective-mass theory of quantum-well absorption treats electron and hole states separately. The spin-$\frac{1}{2}$ electron states are obtained by solving the simple particle-in-a-box model described earlier. (In this calculation the boundary conditions are slightly different since the particle masses are assumed not to vary as the wave function goes from well to barrier. For well widths greater than about 80 Å, this effect is not too important for the lower-lying states.) The effective-mass Hamiltonian for the spin-$\frac{3}{2}$ hole is given by

$$(H_h)_{vv'}=T_{vv'}+V_h(z)\delta_{vv'}\ ,$$

where $v=-\frac{3}{2},\ldots,\frac{3}{2}$ labels the z component of the hole spin. The kinetic-energy matrix $T_{vv'}$ is given in the limit of infinite spin-orbit splitting by the $\mathbf{k}\cdot\mathbf{P}$ expression of Luttinger and Kohn[19] with k_z replaced by the operator $p_z/\hbar$, and the potential energy $V_h(z)$ is a finite square-well potential for the holes. In the multiband effective-mass model the well potential is diagonal in the basis used. It can be shown by detailed tight-binding studies that the off-diagonal components are very small.[20] Strong coupling between heavy- ($v=\pm\frac{3}{2}$) and light- ($v=\pm\frac{1}{2}$) hole subbands results from the off-diagonal components of $T_{vv'}$.

The free-electron and -hole subband states in the envelope-function approximation are

$$|\,\mathbf{k}_{||},n\,\rangle=f_n(z)U_0(\mathbf{r})e^{i\mathbf{k}_{||}\cdot\boldsymbol{\rho}}$$

and

$$|\,\mathbf{k}_{||},m\,\rangle=\sum_v g_m^v(\mathbf{k}_{||},z)U_0^v(\mathbf{r})e^{i\mathbf{k}_{||}\cdot\boldsymbol{\rho}}\ ,$$

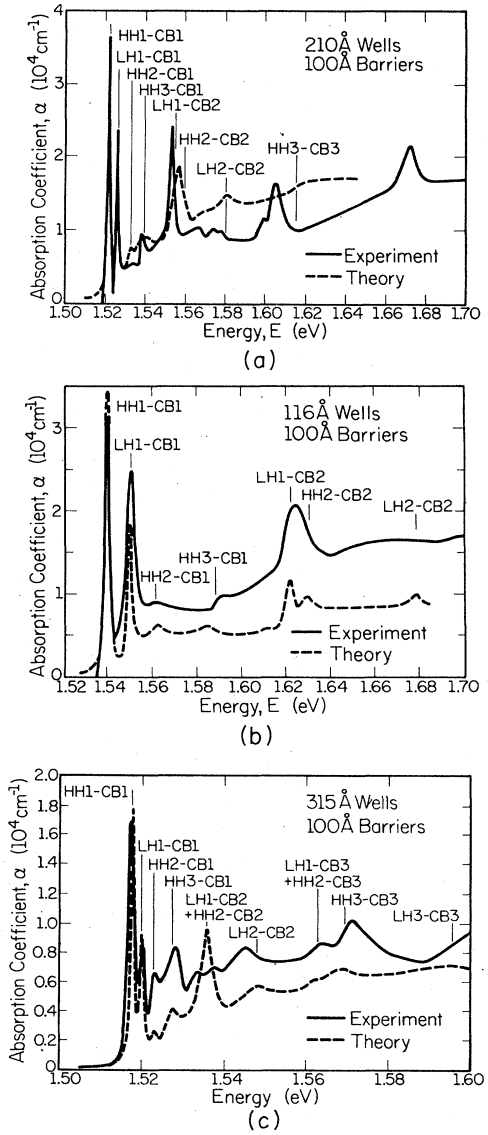

FIG. 3. Measured and calculated absorption spectra of multiple-quantum-well samples with 100-Å barriers with (a) 210-Å wells, (b) 120-Å wells, and (c) 315-Å wells.

respectively. Here, $U_0(\mathbf{r})$ and $U_0^v(\mathbf{r})$ are the zone-center Bloch functions for electrons and holes, and $f_n(z)$ and $g_m^v(z)$ are the corresponding envelope functions, respectively.

The free-carrier problems are solved variationally by expanding the envelope functions in linear combinations of Gaussian basis states; the solutions have been discussed elsewhere.[15,21] Due to the strong coupling between heavy- and light-hole bands, the optical matrix elements are rapidly varying functions of the wave vector $\mathbf{k}_{||}$, and all transitions between different subbands are dipole-allowed.[15,20,22]

The exciton binding energies and envelope functions are obtained by solving a two-dimensional effective-mass equation which incorporates effects of nonparabolic subband structure and valence-band mixing.[15,22] Using Fermi's golden rule one can obtain optical matrix elements and the theoretical absorption spectrum shown in Fig. 3 from the computed effective-mass envelope functions and energies.

The oscillator strength per unit area for light propagating along the growth direction z can be determined by[15,20,22]

$$f_{nm}=\frac{2}{E_g m_0}\left|\sum_{\mathbf{k}_{||}} G_{nm}(\mathbf{k}_{||})\hat{\mathbf{x}}\cdot\mathbf{P}_{nm}(\mathbf{k}_{||})\right|^2 ,$$

where $G_{nm}(\mathbf{k}_{||})$ is the exciton envelope function. In the envelope-function approximation the optical matrix elements $\mathbf{P}_{nm}(\mathbf{k}_{||})$ are given by

$$\mathbf{P}_{nm}(\mathbf{k}_{||})=\sum_v \int d\mathbf{r}\, U_0(\mathbf{r})\mathbf{P}U_0^v(\mathbf{r})\int_{-\infty}^{\infty} dz\, f_n^*(z)g_m^v(\mathbf{k}_{||},z) .$$

The integral involving the Bloch functions is just the optical matrix element between the s-like spin-$\frac{1}{2}$ conduction Bloch state $U_0(\mathbf{r})$ and the p-like spin-$\frac{3}{2}$ Bloch state $U_0^v(\mathbf{r})$, which is proportional to the optical matrix element defined in Ref. 12.

The absorption coefficient for the (n,m)th exciton, $\alpha_{n,m}$, is related to the oscillator strength[23] by

$$\alpha_{n,m}=\frac{4\pi^2 e^2\hbar f_{n,m}}{nmcL}\Delta(\hbar\omega-E_{n,m}) ,$$

where L is the quantum-well width and $\Delta(\hbar\omega-E_{n,m})$ is a Lorentzian function centered on the exciton energy $E_{n,m}$.

The mimic the experimental situation, the band-to-band and exciton-absorption lines are broadened by Lorentzian functions of half-width Γ_b and Γ_x, respectively. The widths Γ_b and Γ_x are chosen to match the experimental data. We have found that reasonable choices for Γ_x and Γ_b are given by $\Gamma_{b,x}=c_0 n_e n_h$ meV, where n_e and n_h are principle quantum numbers for electrons and holes, and c_0 is a dimensionless constant of order unity.[15] In Figs. 3(a)—3(c), c_0 was chosen to be 1, 1, and $\frac{1}{2}$, respectively.

A systematic study of exciton binding energies and oscillator strengths in GaAs-AlGaAs quantum wells has been carried out using the multiband effective-mass model just described. Results of this study are presented in Ref. 22. It is found that valence-band nonparabolicity can increase the exciton binding energy several meV above results obtained in a parabolic approximation. The enhancement in binding energy is most pronounced for those excitons whose valence subbands have negative zone-center effective masses.[15,22] Furthermore, the strong mixing of heavy- and light-hole character leads to a sharing of oscillator strength between $\Delta n=0$ excitons and $\Delta n\neq 0$ excitons, whose valence subbands are nearly degenerate in energy. In particular, the LH1-CB2 exciton is strongly mixed with the HH2-CB2 exciton. Thus the HH2-CB2 $\Delta n=0$ exciton line is predicted to split into a closely spaced pair of exciton lines.[22]

These variationally calculated energies are in good agreement with the Kronig-Penney calculation of Eqs. (1) and (2). As one can see from Fig. 3(a), the agreement is also quite good between these calculated energies and the experimental results.

Figures 3(b) and 3(c) show both the measured and calculated absorption spectra from other multiple-quantum-well structures with 120- and 315-Å wells, respectively. In each of Figures 3(a)—3(c), not only are the transition energies well explained by the calculations, but so are the relative sizes of the transitions. The dominant transitions are, of course, the HH1-CB1 and LH1-CB1 exciton absorption. Also prominent is a peak composed of the superposition of the HH2-CB2 and LH1-CB2 transitions. If there were no mixing of the heavy- and light-hole states, then the LH1-CB2 transition would be forbidden; mixing of the HH2 and LH1 states allows both to contribute. Other experimentally observed transitions which are allowed only because of mixing of the valence bands are HH2-CB1, HH3-CB1, LH1-CB3, and probably HH1-CB5 and HH1-CB6 in Fig. 3(c).

The data of Fig. 3 show that as the well width becomes smaller, the exciton absorption becomes stronger. This trend, which was observed in all of the structures investigated in this study, is explained by our model and is a result of wave-function compression. Figure 4 summarizes the area under the absorption peaks for the $n=1$ heavy- and light-hole excitons. This area, A, is given in units of eV cm^{-1} and is directly proportional to $f_{n,m}/L$ through the relation[23]

$$A_{n,m}=\frac{4\pi^2\hbar e^2 f_{n,m}}{Lm_0 nc} ,$$

where n is the index of refraction of the material, $f_{n,m}$ is the oscillator strength per unit area defined earlier, m_0 is the free-electron mass, and L is the well width. Since $f_{n,m}/L$, the oscillator strength per unit volume, is proportional to $|\phi_{ex}(0)|^2$ [$\phi_{ex}(\mathbf{r})$ is the relative coordinate exciton wave function], we find

$$f_{n,m}/L\propto 1/a^3$$

in a spherically symmetric system with a the exciton Bohr radius. In a quantum well, however, $f_{n,m}/L\propto 1/z\rho^2$, where z is the extent of the exciton in the z direction and ρ is the extent of the exciton in the ρ direction. For narrow wells,[24,25] $z\propto L$ and $\rho\propto L^{1/2}$. Thus, we see

$$A_{n,m}\propto 1/L^2 .$$

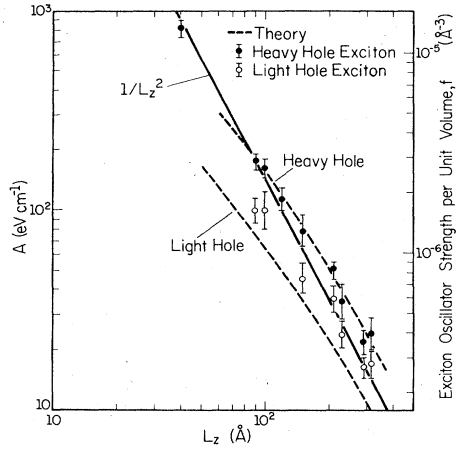

FIG. 4. Integrated absorption intensity A for the $n=1$ heavy-hole and light-hole free excitons as functions of well width and, on the right-hand axis, the oscillator strength f per unit volume. For narrow wells, both A and f are proportional to $1/L^2$; the solid line shows this $1/L^2$ behavior. Also shown are the calculated oscillator strengths per unit volume without any adjustment.

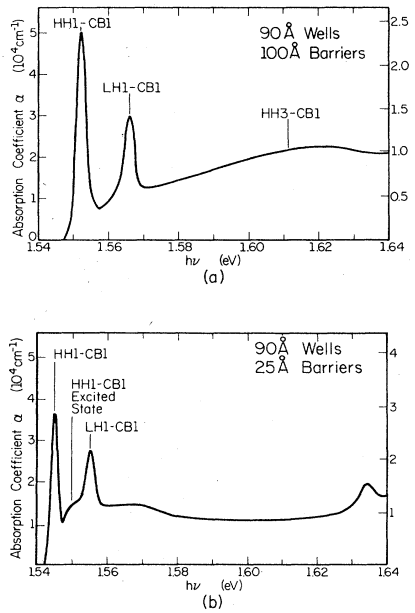

FIG. 5. Absorption spectra of GaAs-$Al_{0.25}Ga_{0.75}As$ multiple-quantum-well samples with 90-Å wells and (a) 100-Å barriers and (b) 25-Å barriers. The arrows point to the calculated location of the various exciton-absorption peaks. The left-hand vertical axis is the absorption coefficient deduced by considering only the wells to contribute to absorption; the right-hand-axis absorption coefficients assume that the entire MQW structure (wells and barriers) contributes to absorption.

For medium-width wells,[24] ρ is about constant, so we deduce that

$$A_{n,m} \propto 1/L \ .$$

For wider wells, even z is about constant, so $A_{n,m}$ is the bulk value. In Fig. 4 we see this behavior for narrow and medium-width wells. Figure 4 also shows the oscillator-strength results from our calculation with no scaling and no adjustable parameters. As is evident from the figure, the agreement is quite good over 2 orders of magnitude. For the heavy-hole exciton, the agreement is almost perfect. The experimental light-hole data are somewhat higher than the calculated results; we believe this is because some of our measured oscillator strength is due to excited states of the heavy-hole exciton.

We have also investigated the effect of well coupling on the absolute absorption coefficients and subband energies. Figure 5(a) depicts the absorption spectrum for a structure with 90-Å wells and 100-Å barriers. The wells in this case are essentially uncoupled. Figure 5(b) shows the absorption spectrum for a structure with 90-Å wells and 25-Å barriers. By comparing these two spectra, we can see some of the effects of wave-function coupling through the barriers. The first and most obvious effect is the lower transition energies in the coupled wells as compared to the uncoupled wells. This is due to the envelope wave functions being less confined in the well and more spherical. This configuration has lower energy.

The transition energies in the coupled wells are successfully predicted from the solutions of Eqs. (2) and (3), as Fig. 5(b) shows. Another important effect of the wave-function coupling is that the absorption strength per well decreases. This is again due to the excitons being more three-dimensional-like than in uncoupled wells.

As discussed earlier, for coupled wells it is not entirely appropriate to consider only the total well thickness for defining the absorption coefficient α. The left-hand vertical axes of Figs. 5(a) and 5(b) shows α defined with the thickness d, the total well thickness, only. On the right-hand vertical axes, α is defined with respect to d, the total superlattice thickness. The left-hand axis label is appropriate for Fig. 5(a) with uncoupled wells; the right-hand axis is perhaps more appropriate for Fig. 5(b) with coupled wells. Even defining α as on the right-hand axis, the superlattice excitons have stronger optical-absorption coefficients than in bulk GaAs.

The effects of coupled wells are seen also in Fig. 6. The structures with 150-Å wells and (a) 100-Å barriers and (b) 25-Å barriers again show the larger oscillator strength in uncoupled wells than in coupled wells. [The transition energies in this case are about the same in (a) and (b); this is because the structure depicted in (b) has slightly narrower wells than that of (a).]

An additional interesting effect seen in Fig. 6 is the apparent enhancement of the HH3-CB1 oscillator strength of the coupled wells over the uncoupled wells. If this is a real effect, it could be explained by two mechanisms. (1) In the coupled wells, the HH3 and LH1 levels are closer to each other, leading to more mixing and therefore an enhanced oscillator strength of this "forbidden" transi-

tion. (2) Even ignoring valence-band mixing, in the coupled wells the electron wave functions are more strongly coupled from well to well than are the hole wave functions. Thus the labeling is not really the same for electrons and holes, leading to some nonorthogonality of HH3 and CB1 even without valence-band mixing.

Finally, it is possible that the transition only appears to be enhanced because the continuum absorption near the HH3-CB1 transition has been decreased due to Fano-resonance effects.[26] Especially in Fig. 6(b), the continuum absorption near the HH3-CB1 exciton absorption appears depressed. It is also not unreasonable that the Fano-resonance effect would differ between these two cases of coupled and uncoupled wells. The interaction between a discrete state and a two-dimensional continuum will probably be weaker than that between a discrete state and a quasi-three-dimensional continuum; this would lead to a enhanced Fano resonance in the coupled wells.

In conclusion, the absolute absorption spectra for AlGaAs-GaAs multiple-quantum-well structures with both coupled and uncoupled wells have been measured. These results are well explained within our described theoretical models. We observe a large number of absorption peaks, many of which are due to $\Delta n \neq 0$ "forbidden" transitions. These transitions are, in fact, allowed because of valence-band hybridization, and their appearance and oscillator strengths agree well with a theoretical model which includes this effect.

Oscillator strengths for the excitons in quantum wells are stronger than for excitons in bulk GaAs. The oscillator strength increases with decreasing well width due to exciton confinement and is in good agreement with our calculations. For well widths of less than 150 Å, the oscillator strength per unit volume varies as $1/L^2$. Finally, we show that the effect of coupling between adjacent quantum wells is to lower both the subband energies and the oscillator strengths.

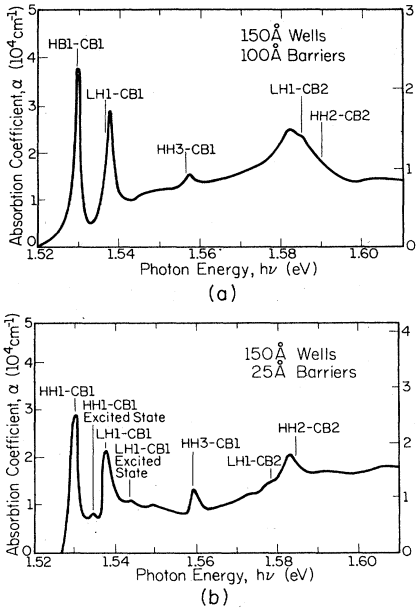

FIG. 6. Absorption spectra of GaAs-$Al_{0.25}Ga_{0.75}As$ multiple-quantum-well samples with 150-Å wells and (a) 100-Å barriers and (b) 25-Å barriers. The arrows point to the calculated location of the various exciton-absorption peaks. The left-hand vertical axis is the absorption coefficient deduced by considering only the wells to contribute to absorption; the right-hand-axis absorption coefficients assume that the entire MQW structure (wells and barriers) contributes to absorption.

ACKNOWLEDGMENTS

This work was supported by the Joint Services Electronics Program, the Air Force Office of Scientific Research, and by the Office of Naval Research (under Contract No. N00014-81-K-0430). The authors acknowledge useful discussions with Professor M. V. Klein. One of us (W.T.M.) was supported by IBM.

*Also at Department of Physics, University of Illinois at Urbana-Champaign, Urbana, IL 61081.

†Also at Department of Electrical and Computer Engineering, University of Illinois at Urbana-Champaign, Urbana, IL 61801.

‡Also at Department of Metallurgy and Mining, University of Illinois at Urbana-Champaign, Urbana, IL 61801.

[1]R. Dingle, in *Festkörperprobleme (Advances in Solid State Physics)*, edited by H. J. Queisser (Pergamon-Vieweg, Braunschweig, 1975), Vol. 15, pp. 21–48.

[2]R. Dingle, W. Wiegmann, and C. H. Henry, Phys. Rev. Lett. **33**, 827 (1974).

[3]R. Dingle, A. C. Gossard, and W. Wiegmann, Phys. Rev. Lett. **34**, 1327 (1975).

[4]R. Tsu, L. L. Chang, G. A. Sai-Halasz, and L. Esaki, Phys. Rev. Lett. **34**, 1509 (1975).

[5]R. Dingle, in *Festkörperprobleme (Advances in Solid State Physics)*, Ref. 1, Vol. 15, p. 39.

[6]R. C. Miller, D. A. Kleinman, W. T. Tsang, and A. C. Gossard, Phys. Rev. B **24**, 1134 (1981).

[7]J. C. Maan, G. Belle, A. Fasolino, M. Altarelli, and K. Ploog, Phys. Rev. B **30**, 2253 (1984).

[8]S. Tarucha, H. Okamoto, Y. Iwasa, and N. Miura, Solid State Commun. **52**, 815 (1984).

[9]D. A. B. Miller, D. S. Chemla, T. C. Damen, A. C. Gossard, W. Wiegmann, T. H. Wood, and C. A. Burrus, Phys. Rev. Lett. **53**, 2173 (1984).

[10]T. Henderson, W. Kopp, R. Fischer, J. Klem, H. Morkoç, L. P. Erickson, and P. W. Palmberg, Rev. Sci. Instrum. **55**, 1763 (1984).

[11]H. C. Casey, Jr. and M. B. Panish, *Heterostructure Lasers* (Academic, New York, 1978), Pt. A, p. 192.

[12]P. Lawaetz, Phys. Rev. B **4**, 3460 (1971).

[13]D. Arnold, A. Ketterson, T. Henderson, J. Klem, and H. Morkoç, Appl. Phys. Lett. **45**, 1237 (1984).

[14]H. Okumura, S. Misawa, S. Yoshida, and S. Gonda, Appl. Phys. Lett. **46**, 377 (1985).

[15]G. D. Sanders and Y. C. Chang, Phys. Rev. B **31**, 6892 (1985).

[16]J. I. Pankove, *Optical Processes in Semiconductors* (Dover, New York, 1975), Chap. 3.

[17]H. C. Casey, Jr., D. D. Sell, and M. B. Panish, Appl. Phys. Lett. **24**, 63 (1974).

[18]D. D. Sell and H. C. Casey, Jr., J. Appl. Phys. **45**, 800 (1974).

[19]J. M. Luttinger and W. Kohn, Phys. Rev. **97**, 869 (1956).

[20]Y. C. Chang and J. N. Schulman, Appl. Phys. Lett. **43**, 536 (1983); Phys. Rev. B **31**, 2069 (1985).

[21]A. Fasolina and M. Altarelli, *Two-Dimensional Systems, Heterostructures and Superlattices* (Springer, Berlin, 1984), p. 176.

[22]G. D. Sanders and Y. C. Chang, Phys. Rev. B **32**, 5517 (1985).

[23]F. Bassani and G. P. Parravicini, *Electronic States and Optical Transitions in Solids* (Pergamon, Oxford, 1975), Chap. 5.

[24]G. Bastard, E. E. Medez, L. L. Chang, and L. Esaki, Phys. Rev. B **26**, 1974 (1982).

[25]J. M. Rorison and D. C. Herbert, in Proceedings of the International Conference on Superlattices, Microstructures, and Microdevices, Urbana-Champaign, 1984 [Superlattices Microstruct. (to be published)].

[26]U. Fano, Phys. Rev. **124**, 1866 (1961).